



# Cone-type multi-directional viewing-zone extension of a computer-generated hologram via a shuffle interconnection

SOOBIN KIM,<sup>1</sup> YOUNG-JU KIM,<sup>2</sup> TAEONE KIM,<sup>3</sup> AND HWI KIM<sup>1,\*</sup> 

<sup>1</sup>*Department of Electronics and Information Engineering, College of Science and Technology, Korea University, Sejong-Campus, 2511 Sejong-ro, Sejong 30019, Republic of Korea*

<sup>2</sup>*Yuman Optics Inc., 1 Bucheon-ro 419beon-gil, Bucheon-si, Gyeonggi-do 14454, Republic of Korea*

<sup>3</sup>*5G Giga Communication Research Laboratory, Electronics and Telecommunications Research Institute, 218 Gajeong-ro Yuseong-gu Daejeon 34129, Republic of Korea*

\*[hwikim@korea.ac.kr](mailto:hwikim@korea.ac.kr)

**Abstract:** We propose the multi-directional viewing-zone extension of computer-generated holograms (CGHs) using a single flat-panel spatial light modulator (SLM) and a multi-directional shuffle interconnection. A design breaking the SLM plane into several sub-zone regions and creating extended viewing-zones through a multi-directional shuffle interconnection is presented with a proof-of-concept experiment generating a cone-like viewing zone subtended by sixteen sub-viewing-zones.

© 2022 Optica Publishing Group under the terms of the [Optica Open Access Publishing Agreement](#)

## 1. Introduction

The three-dimensional (3D) holographic display has recently attracted wide interest as the ultimate 3D display technology [1–7]. Even in state-of-the-art holographic 3D display development, however, the eye-box is severely limited to a single small viewing zone through which the viewer can perceive the holographic accommodation effect of holographic 3D images. The size of the viewing zone is determined by the pixel size of the SLM [8,9] and most of conventional SLMs have a narrow viewing zone.

Dynamic time-domain techniques such as eye-tracking and gaze-tracking have been actively developed for eye motion box (EMB) extension. Recently, Y. Lim et al. reported the state-of-the-art 360-degree full-color holographic table-top display using fast MEMS SLMs robustly synchronized to rotating mechatronics [1]. However, non-mechanical EMB extension is still strongly needed. Recently an exceptional 1 $\mu$ m pixel size reflection type liquid crystal on silicon (LCoS) SLM prototype was announced and is at the laboratory stage of development [10,11]. It was shown that random-pattern encoded CGH can provide viewing zone extension. The random pinhole sieve and random phase plate attached to SLM have been tested for extending the viewing zone [12]. This method re-distributes, under space-bandwidth-product (SBP) invariance, the information capacity in the resolution of SLM for the bandwidth extension of the spatial-frequency domain, which means the EMB extension.

The technique of random-pattern based re-distribution of the SLM data capacity increases noise-levels due to the random nature of the method. Furthermore, the image quality is extremely sensitive to the optical alignment of the SLM and additional random modulation plates. The system cannot tolerate even slight miss-alignment of the incidence direction of the light source and fabrication misalignment [12,13].

In this paper, we propose a method for the redistribution of SLM data capacity to extend the EMB without using the random pattern method. The multi-directional shuffle interconnection is devised to distribute several sub-zone regions of a SLM into multi-directional viewing zones. A proof-of-concept experiment is performed, in which a high-resolution flat panel SLM is channeled to a cone-like sixteen times extended viewing-zone displaying sixteen CGH images. In section 2,

the system design concept is described. In section 3, the experimental results of multi-directional CGHs are presented alongside a numerical simulation, and the concluding remarks follow.

## 2. System design and CGH synthesis

The concept of the proposed multi-directional shuffle interconnection system is illustrated in Fig. 1. Without loss of generality, we describe the design of a 16-channel multi-directional shuffle interconnecting system. As seen in Fig. 1, the entire area of the SLM is divided into  $4 \times 4$  sub-zones. The directional shuffle interconnector performs the mapping of the sixteen sub-zones to the circular-symmetric viewing-zones. The finite overlap volume of the sixteen directional beam lines specifies a common holographic image volume space. The viewer watches the CGH image through the viewing zones on the circumference. Generally, the multi-directional shuffle interconnector can be extended to an N channel system. As a proof-of-concept, we present the design and experimental results of a 16-channel system.

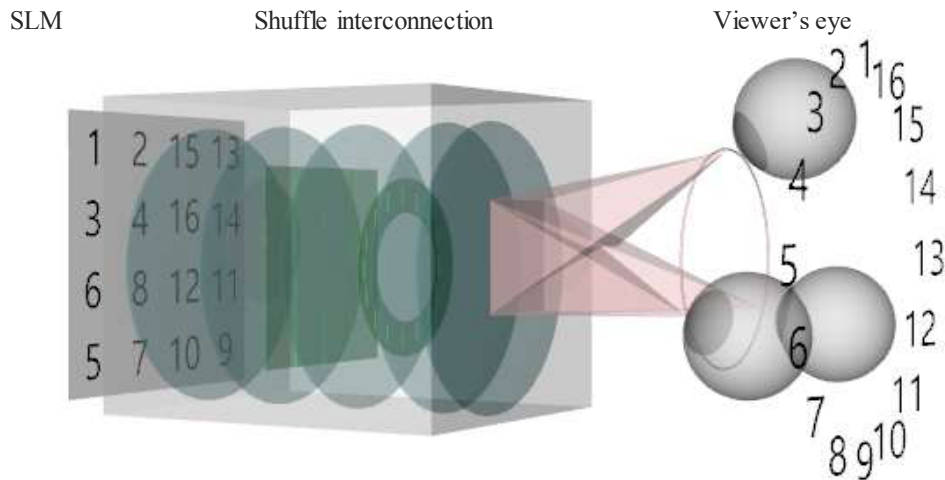


**Fig. 1.** Schematic diagram of the multi-directional shuffle interconnecting system

Figure 2 presents the system design of a 16-channel viewing-zone. An amplitude SLM is placed at the  $x_1y_1$  plane and the first  $4f$  system that consists of 0.2m focal length lenses ( $L_1, L_2$ ) with a spatial filter at the  $u_1v_1$  plane that performs single-side band filtering to form a virtual complex SLM image at the  $x_2y_2$  plane. A prism-array plate shown in Fig. 2(b) is put in the  $x_2y_2$  plane to modulate the carrier waves of the sub-zones of the complex SLM. The first square prism-array  $F(x_2, y_2)$  is designed to interconnect the sixteen beam lines to the second prism array  $G(u_2, v_2)$  at the  $u_2v_2$  plane through lens  $L_3$ .

The second prism array takes the form of a prism annulus, as shown in Fig. 2(c). It corrects the directions of the sixteen beam lines at the annulus to form an overlap image volume space at the field lens through lens  $L_4$  and the sixteen focused viewing zones through the field lens  $L_5$  at the circular circumference of the eye lens plane. As a consequent, the sixteen viewing zones are formed along a circle of 30mm radius, with the vertical viewing angle at each viewpoint being 2.29 degrees from the optical axis. This configuration eventually makes an overlap volume space at the field lens plane. The ray tracing in Fig. 2(a) calculated by ZEMAX simulation shows the streamline of the optical fields.

The square prism shown in Fig. 2(b) with sides 40mm long is composed of sixteen sub prisms with 7.07mm side lengths. The annulus prism of 20mm radius is composed of sixteen sub-prisms with 5.55mm side lengths. Each sub prism is rotated to collimate the incident rays parallel to the

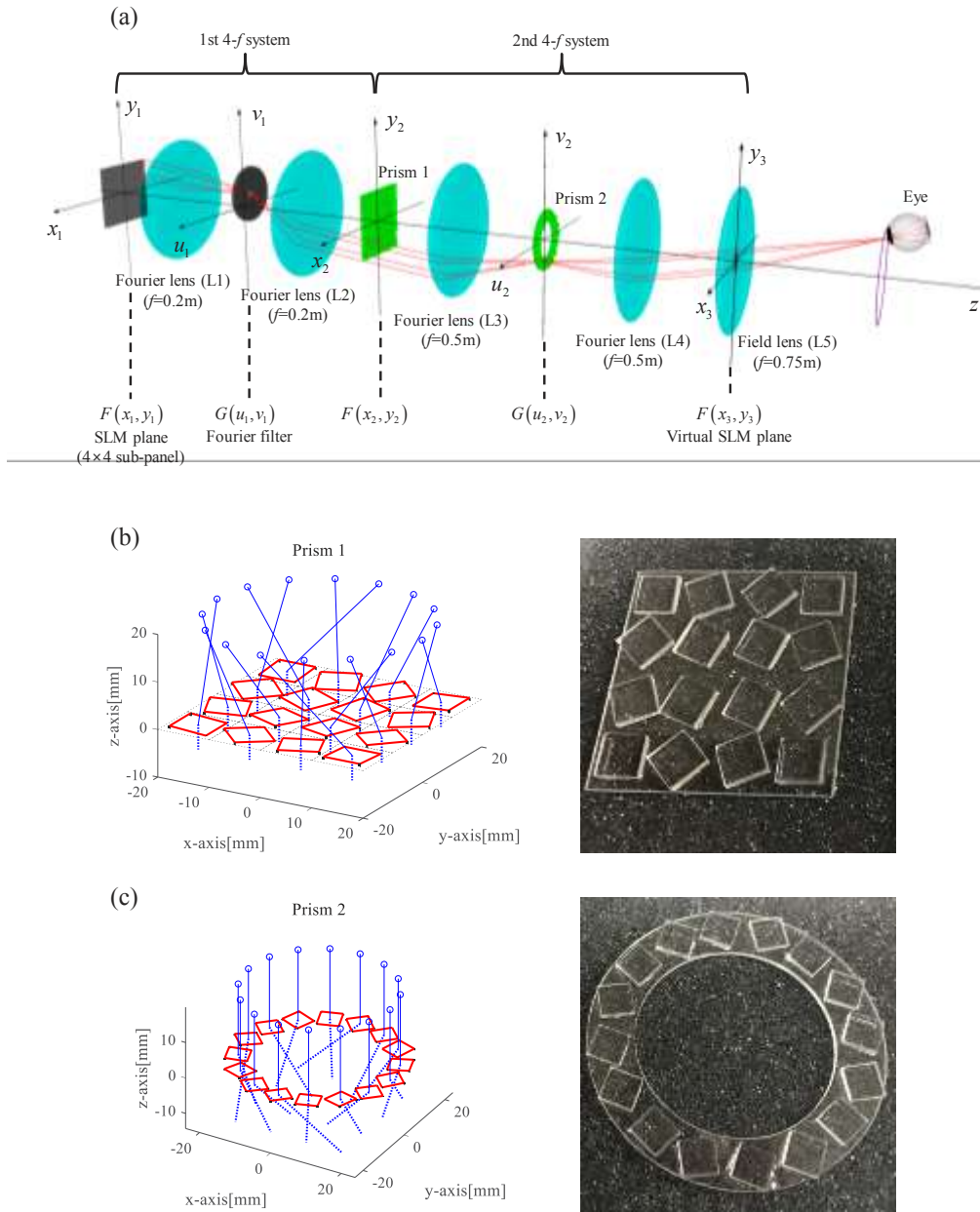


**Fig. 2.** System design of the multi-directional shuffle interconnecting system. (a) Schematics with ZEMAX ray-tracing analysis, the design and fabrication of (b) the first prisms array  $F(x_2, y_2)$  and the second prism array  $G(u_2, v_2)$

optical axis, as presented in Fig. 2(c). The system parameters of the designed multi-directional shuffle interconnecting system are presented in Table 1.

**Table 1. Parameters of the components for the proposed system (Fig. 2)**

Component	Parameter
Panel	704 × 704, (sub panel = 176 × 176), 56.7μm
Focal length of L1 and L2	0.2m
Focal length of L3 and L4	0.5m
Focal length of L5	0.75m
Size of prism 1	40mm × 40mm
Size of sub prism 1	7.07mm × 7.07mm
Tilt angle of prism 1	4.34°
Radius of prism 2	20mm (in; 16mm, out; 24mm)
Size of sub prisms 2	5.55mm
Tilt angle of prism 2	4.66°, 3.5°, 1.56°

The wave optic description of the multi-directional shuffle interconnector is necessary to synthesize the directional CGH patterns. The relationship between the field at the square prism and the annulus prism through lens  $L_3$  is given as

$$G(u_2, v_2) = \frac{e^{jk_2f}}{j\lambda f} \int_{-\infty}^{\infty} \int_{-\infty}^{\infty} F(x_2, y_2) \exp \left[ \frac{-j2\pi}{\lambda f} (x_2 u_2 + y_2 v_2) \right] dx_2 dy_2, \quad (1)$$

where  $F(x_2, y_2) = \sum_m F_m(x_2 - x_m, y_2 - y_m)$  and  $G(u_2, v_2) = \sum_m G_m(u_2 - u_m, v_2 - v_m)$ .

The  $m$ th sub-zone is located at  $(x_m, y_m)$  on the square array. If we insert the square prism for the sub-zone in front of the virtual SLM plane,

$$P(x_2, y_2) = \sum_m P_m(x_2 - x_m, y_2 - y_m), \text{ where } P_m(x, y) = \exp \left[ \frac{j2\pi}{\lambda f} (xu_m + yv_m) \right]$$

The Fourier transformed field of the  $m$ th sub-zone

$T(x_2, y_2) = \sum_m F_m(x_2 - x_m, y_2 - y_m) P_m(x_2 - x_m, y_2 - y_m)$  is obtained as

$$\begin{aligned} G_m(u_2, v_2) &= \frac{e^{jk_2f}}{j\lambda f} \int_{-\infty}^{\infty} \int_{-\infty}^{\infty} P_m(x_2 - x_m, y_2 - y_m) F_m(x - x_m, y - y_m) \exp \left[ \frac{-j2\pi}{\lambda f} (xu_2 + yv_2) \right] dx dy \\ &= \exp \left[ \frac{-j2\pi}{\lambda f} (x_m u_2 + y_m v_2) \right] \frac{e^{jk_2f}}{j\lambda f} \int_{-\infty}^{\infty} \int_{-\infty}^{\infty} \exp \left[ \frac{j2\pi}{\lambda f} (x_2 u_m + y_2 v_m) \right] F_m(x_2, y_2) \exp \left[ \frac{-j2\pi}{\lambda f} (x_2 u_2 + y_2 v_2) \right] dx_2 dy_2 \\ &= \exp \left[ \frac{-j2\pi}{\lambda f} (x_m u_2 + y_m v_2) \right] g_m(u_2 - u_m, v_2 - v_m) \end{aligned} \quad (2)$$

where  $g_m(u_2, v_2) = \frac{e^{jk_2f}}{j\lambda f} \int_{-\infty}^{\infty} \int_{-\infty}^{\infty} F_m(x, y) \exp \left[ \frac{-j2\pi}{\lambda f} (xu_2 + yv_2) \right] dx dy$ . To arrange the array of signals as a circle in the  $(u_2, v_2)$  plane, the  $(u_m, v_m)$  pair is defined by

$$u_m = R \times \cos \left( \frac{2\pi}{N_v} m \right) \quad (3)$$

$$v_m = R \times \sin \left( \frac{2\pi}{N_v} m \right) \quad (4)$$

where  $R$  is 20mm, the radius of circular prism, and  $N_v$  is 16, representing the number of viewing windows. The resulting square prisms array is presented in Fig. 2(b).

In the local coordinate of the Fourier plane at  $(u_m, v_m)$ , the transmittance function of the local circular prism giving carrier waves to cancel out the phase of  $G_m(u_2, v_2)$  is defined by

$$C_m(u_2, v_2) = \exp \left[ \frac{j2\pi}{\lambda f} (u_2 x_m + v_2 y_m) \right]. \quad (5)$$

Then, the modulated field distribution in  $(u_m, v_m)$  plane is modeled by

$$G_m(u_2, v_2)C_m(u_2, v_2) = g_m(u_2 - u_m, v_2 - v_m) \quad (6)$$

The aim of the circular prism is to converge the sub-panel field to the optical axis in the field lens plane  $(x_3, y_3)$ . The design and fabricated circular prism array are presented in Fig. 2(c). The virtual plane of the 2nd 4f system,  $W_m(x_3, y_3)$  is represented by

$$\begin{aligned} W_m(x_3, y_3) &= \frac{e^{j2kf}}{j\lambda f} \int_{-\infty}^{\infty} \int_{-\infty}^{\infty} g_m(u_2 - u_m, v_2 - v_m) \exp \left( \frac{-j2\pi}{\lambda f} (x_3 u_2 + y_3 v_2) \right) du_2 dv_2 \\ &= \frac{e^{j2kf}}{j\lambda f} \exp \left( \frac{-j2\pi}{\lambda f} (x_3 u_m + y_3 v_m) \right) \int_{-\infty}^{\infty} \int_{-\infty}^{\infty} g_m(u_2, v_2) \exp \left( \frac{-j2\pi}{\lambda f} (x_3 u_2 + y_3 v_2) \right) du_2 dv_2 \\ &= \frac{e^{j2kf}}{j\lambda f} \exp \left( \frac{-j2\pi}{\lambda f} (x_3 u_m + y_3 v_m) \right) F_m(x_3, y_3). \end{aligned} \quad (7)$$

Consequently, the proposed multi-directional shuffle interconnecting system delivers the sub-zone  $F_m(x_2 - x_m, y_2 - y_m)$  in the  $(x_2, y_2)$  plane to form the directional image field,  $\exp \left( \frac{-j2\pi}{\lambda f} (x_3 u_m + y_3 v_m) \right) F_m(x_3, y_3)$  in the  $(x_3, y_3)$  plane.

We can deliver a complex CGH image to the viewer along the sixteen channels. The viewer has sixteen viewing zones on a circular circumference shape. The CGH is synthesized by the inverse cascaded Fresnel transform [15].

### 3. Experimental results

We experimentally demonstrate the proposed multi-directional shuffle interconnection system for sixteen view CGH contents. Figure 3 presents the experimental schematic of the proposed system and the implementation of the testbed.

The first 4-f system uses a convex lens of focal length 0.2m and the square prism is placed on the virtual SLM plane. The first 4-f system performs the single side-band filter transforming the amplitude CGH on the SLM to the complex CGH pattern behind the square prism [16]. The second 4-f system (Lens4) performs the optical Fourier transform from the circular prism plane to the field lens plane (Lens5). The lens of the second 4-f system is a convex lens with a focal length of 0.5m. At the field lens plane, the SLM generate sixteen directional CGH images. The field lens with a focal length 0.75m allows sixteen viewing zones in the viewer's eye plane. The viewer's eye motion box is circular in shape revolving 360 degrees around the optical axis, as illustrated in Fig. 1.

The key part of the proposed system is two prism-type phase plates. The prism refractive index is 1.52, and the fabrication tolerance is about  $\pm 0.005$ mm. The light source is a 660nm solid-state laser (06-06-MLD, Cobolt) and it is collimated to an expanded plane wave using an expander (BE02-05-A, Thorlabs). In practice, the central part with  $706 \times 706$  resolution of the SLM, which has a pixel size of  $56.7 \mu\text{m}$ , is selectively used, and the resolution of the sub-zones is set at  $176 \times 176$ . The focal length of the field lens is 0.75m. The 16-channel target image and its CGH pattern are shown in Figs. 3(c) and 3(d). Figure 3(e) presents the experimental observation of the multi-directional shuffle interconnection of the sixteen numbers on the square amplitude SLM to the sixteen directional images.

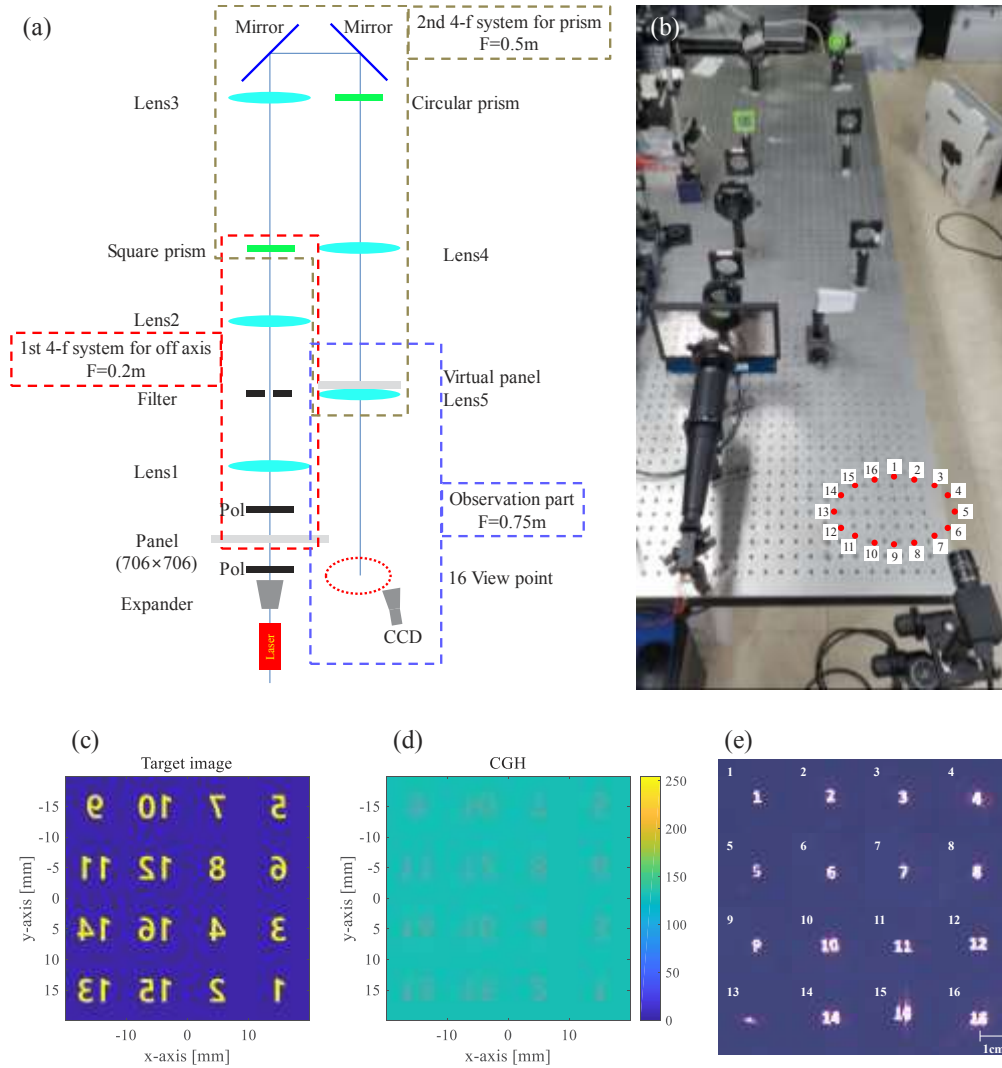


**Fig. 3.** (a) Schematic diagram and (b) testbed for optical experiment. (c) Target sixteen view images, (d) CGH and (e) sixteen view observation results.

The single side band amplitude CGH synthesis [14] is employed to generate a CGH pattern (Fig. 4(a)). Representing the accommodation effect, Fig. 4 presents ‘5’ sub-zone CGH images delivered to the corresponding 5th viewing zone.

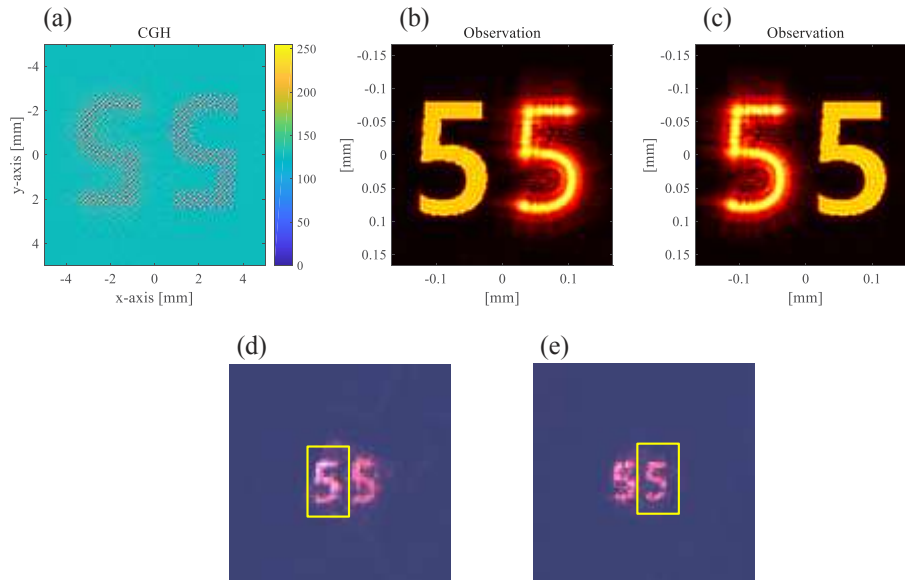


**Fig. 4.** (a) CGH pattern, and the simulation results for observation of focusing on (b) left “5” and (c) right “5”, and experimental observation of focusing on (d) left “5” and (e) right “5”.

Finally, we experimented separately to confirm an accommodation effect. The experimental results for the accommodation effect are presented in Figs. 4(b) and 4(e), which show the result of focusing on the right ‘5’ from the distance of 300mm and the left ‘5’ from the distance of 1mm from the virtual panel plane. In the holographic display development, many research directions, such as those associated with continuous viewpoints, resolution enhancement, or field-of-view enhancement, EMB extension, remain to be explored.

In principle, the SLM could be composed of tiled sub-SLMs with non-negligible bezels. Instead of dividing a single SLM into multiple sub-zones, multiple SLMs could comprise a high-resolution multi-vision, thereby enhancing the resolution of the single directional CGH. In the present structure, prism1 and prism2 are static, so discrete directional views are generated. However, if prism1 worked as a dynamic LC prism array and prism2 was rotatable in the time domain, we could expect a continuous viewing zone along the circumference of the cone. For instance, assuming we use an 8K resolution SLM with  $4 \times 4$  division, if prism1 was a dynamic prism and prism2 is rotating by  $22.5(\text{deg.})$ , we could obtain a continuous cone-type viewing zone. For each direction, the viewer could see a 2K resolution CGH. Adjustment of the focal length of the second 4F system could lead to changes in the cone-angle. If the cone-angle reaches  $45(\text{deg.})$ , the display becomes a table-top holographic display while, narrowing the cone-angle down to a single pupil would maximize the holographic accommodation effect. If we select two views on the circumference fit for viewers’ left and right eyes and use a  $2 \times 1$  division in the SLM plane with appropriately designed guiding prisms, we can realize a binocular holographic display.

#### 4. Conclusion

In conclusion, we have proposed a multi-directional shuffle interconnection enabling the multi-directional viewing-zone extension of CGHs. Although we present a 16-view multi-directional

CGH image due to the practical limitations, the proposed concept can be straightforwardly extended to large scale multi-directional applications. It is believed that the extended version of this structure could be employed to construct 360-degree table top multi-view holographic displays.

**Funding.** Korea University Grant.

**Disclosures.** The authors declare no conflicts of interest.

**Data availability.** Data underlying the results presented in this paper are not publicly available at this time but may be obtained from the authors upon reasonable request.

## References

1. Y. Lim, K. Hong, H. Kim, H.-E. Kim, E.-Y. Chang, S. Lee, T. Kim, J. Nam, H.-G. Choo, J. Kim, and J. Hahn, "360-degree tabletop electronic holographic display," *Opt. Express* **24**(22), 24999–25009 (2016).
2. T. Kakue, T. Nishitsuji, T. Kawashima, K. Suzuki, T. Shimobaba, and T. Ito, "Aerial projection of three-dimensional motion pictures by electro-holography and parabolic mirrors," *Sci. Rep.* **5**(1), 11750 (2015).
3. Y. Takaki and S. Uchida, "Table screen 360-degree three-dimensional display using a small array of high-speed projectors," *Opt. Express* **20**(8), 8848–8861 (2012).
4. Y. Takaki and J. Nakamura, "Generation of 360-degree color three-dimensional images using a small array of high-speed projectors to provide multiple vertical viewpoints," *Opt. Express* **22**(7), 8779–8789 (2014).
5. T. Inoue and Y. Takaki, "Table screen 360-degree holographic display using circular viewing-zone scanning," *Opt. Express* **23**(5), 6533–6542 (2015).
6. X. Xia, X. Liu, H. Li, Z. Zheng, H. Wang, Y. Peng, and W. Shen, "A 360-degree floating 3D display based on light field regeneration," *Opt. Express* **21**(9), 11237–11247 (2013).
7. S. Yoshida, "fVisiOn: 360-degree viewable glasses-free tabletop 3D display composed of conical screen and modular projector arrays," *Opt. Express* **24**(12), 13194–13203 (2016).
8. P. S. Hilaire, S. A. Benton, M. Lucente, J. D. Sutter, and W. J. Plesniak, "Advances in holographic video," *Proc. SPIE* **1914**, 188–196 (1993).
9. R. Haussler, S. Reichelt, N. Leister, E. Zschau, R. Missbach, and A. Schwerdtner, "Large real-time holographic displays: from prototypes to a consumer product," *Proc. SPIE* **7237**, 72370S (2009).
10. J. H. Choi, J. H. Yang, J. E. Pi, C. Y. Hwang, Y. H. Kim, G. H. Kim, H. O. Kim, and C. S. Hwang, "The new route for realization of 1- $\mu$ m-pixel-pitch high-resolution displays," *SID Int. Symp. Digest Tech. Papers* **50**(1), 319–321 (2019).
11. C.-S. Hwang, Y.-H. Kim, J. Choi, J.-E. Pi, G. Kim, J.-H. Yang, C.-Y. Hwang, J. Kim, H.-O. Kim, W.-J. Lee, K.-H. Lee, S.-H. Ko Park, and J. Kim, "Achieving 1 $\mu$ m pixel pitch display for electronic holography," *Proc. SPIE* **11304**, 113040L (2020).
12. J. Park, K. Lee, and Y. Park, "Ultrathin wide-angle large-area digital 3D holographic display using a non-periodic photon sieve," *Nat Commun* **10**(1), 1304 (2019).
13. W.-Y. Choi, C.-J. Lee, B.-S. Kim, K.-J. Oh, K. Hong, H.-G. Choo, J. Park, and S.-Y. Lee, "Numerical analysis on a viewing angle enhancement of a digital hologram by attaching a pixelated random phase mask," *Appl. Opt.* **60**(4), A54–A61 (2021).
14. H. Kim, C.-Y. Hwang, K.-S. Kim, J. Roh, W. Moon, S. Kim, B.-R. Lee, S. Oh, and J. Hahn, "Anamorphic optical transformation of an amplitude spatial light modulator to a complex spatial light modulator with square pixels [invited]," *Appl. Opt.* **53**(27), G139–G146 (2014).
15. J. Roh, K. Kim, E. Moon, S. Kim, B. Yang, J. Hahn, and H. Kim, "Full-color holographic projection display system featuring an achromatic Fourier filter," *Opt. Express* **25**(13), 14774–14782 (2017).
16. E. CuChe, P. Marquet, and C. Depeursinge, "Spatial filtering for zero-order and twin-image elimination in digital off-axis holography," *Appl. Opt.* **39**(23), 4070–4075 (2000).